Geomechanics and Engineering, *Vol. 31, No. 3 (2022) 291-304*
https://doi.org/10.12989/gae.2022.31.3.291

Prediction of maximum shear modulus (G_{max}) of granular soil using empirical, neural network and adaptive neuro fuzzy inference system models

Alireza Hajian[1a] and Meysam Bayat*[2]

[1]*Department of Physics, Najafabad Branch, Islamic Azad University, Najafabad, Iran*
[2]*Department of Civil Engineering, Najafabad Branch, Islamic Azad University, Najafabad, Iran*

(*Received April 3, 2022, Revised October 27, 2022, Accepted October 31, 2022*)

Abstract. Maximum shear modulus (G_{max} or G_0) is an important soil property useful for many engineering applications, such as the analysis of soil-structure interactions, soil stability, liquefaction evaluation, ground deformation and performance of seismic design. In the current study, bender element (BE) tests are used to evaluate the effect of the void ratio, effective confining pressure, grading characteristics (D_{50}, C_u and C_c), anisotropic consolidation and initial fabric anisotropy produced during specimen preparation on the G_{max} of sand-gravel mixtures. Based on the tests results, an empirical equation is proposed to predict G_{max} in granular soils, evaluated by the experimental data. The artificial neural network (ANN) and Adaptive Neuro Fuzzy Inference System (ANFIS) models were also applied. Coefficient of determination (R^2) and Root Mean Square Error (RMSE) between predicted and measured values of G_{max} were calculated for the empirical equation, ANN and ANFIS. The results indicate that all methods accuracy is high; however, ANFIS achieves the highest accuracy amongst the presented methods.

Keywords: ANFIS; bender element; gravel; maximum shear modulus; MLP; sand

1. Introduction

Maximum shear modulus or small-strain ($\leq 10^{-3}$%) dynamic shear modulus, G_{max}, is a key parameter in geotechnical design and analysis of geotechnical structures, composite materials, soil-structure interaction problems and estimation of geotechnical parameters (Bosiljkov *et al.* 2005, Cha and Cho 2007, Chang and Cho 2010, Cho *et al.* 2018, Clayton 2011, Liang *et al.* 2018, Oh *et al.* 2017, Yang and Yan 2009). At small shear strain ranges, the behavior of soils is mostly elastic. In elastic theory, Gmax is commonly obtained by in situ and/or laboratory determined shear wave velocity ($G_{max} = \rho . V_s^2$).

Granular soil is defined as a soil containing gravel, sand, or silt with little or no clay content. The texture of granular soil is mainly coarse particles and has no cohesive strength. Coarse granular soils are extensively used in the construction of large earth dams and massive fills due to the well-recognized mechanical characteristics of these types of materials. Recent studies indicated that G_{max} or V_s of granular soils is a function of grading characteristics, effective confining pressure, void ratio, pore structure of soil, initial fabric and loading characteristics (Bayat and Ghalandarzadeh 2018, 2019, El Mosallamy *et al.* 2016, Goudarzy *et al.* 2017, Hussien and Karray 2016, Li 2011, Ruan *et al.* 2021, Teachavorasinskun and Pongvithayapanu 2016, Yu and Richart 1984, Zhou *et al.* 2018, Zhu *et al.* 2014).

A variety of advanced laboratory techniques such as the bender element (BE), ultrasonic and Resonant Column (RC) are nowadays employed to measure small strain stiffness of soil specimens (Carette and Staquet 2016, Senetakis and Payan 2018, Xiao *et al.* 2018). A typical piezoceramic BE is an electromechanical transducer which can generate or receive shear waves in laboratory testing (Shirley 1978). The shear strain levels induced by a BE testing are in the order of 10^{-5} (Dyvik and Madshus 1986). The RC apparatus is used in research and commercial laboratories to measure the dynamic properties of soil across the small to medium strain range. Gu and Yang (2011) indicated that the RC apparatus is the most reliable laboratory method for measurement of small strain shear modulus. Previous studies found good agreement between small strain stiffness values from BE and RC tests for granular soil (Gu *et al.* 2013, Youn *et al.* 2008). So far, several empirical equations have been proposed to predict the G_{max} of granular soil. Hardin's equation is widely used for estimation of G_{max} in granular soils which is given below (Hardin and Black 1967, Hardin and Richart 1963)

$$G_{\max} = AF(e)(\sigma'_m)^n \quad (1)$$

where σ'_m is mean effective confining stress which is defined as $\frac{\sigma_1 + 2\sigma_3}{3}$, $F(e)$ is void ratio function describing the effects of e on G_{max}; A and n are model parameters depending on the grain size distribution (Wichtmann *et al.* 2015). In the previous studies, stress exponent n varies from 0.12 to 0.57 (Li 2016) and also, different forms of $F(e)$ were proposed. Hence, there is no universal *F(e) as a global function* for the whole types of granular soil under different conditions.

*Corresponding author, Assistant Professor
E-mail: bayat.m@pci.iaun.ac.ir
[a]Associate Professor

ISSN: 2005-307X (Print), 2092-6219 (Online)

The recent decade researches indicated that Adaptive Neuro Fuzzy Inference System (ANFIS) and artificial neural network (ANN) as data-based approaches are useful tools for prediction of mechanical, dynamic parameters of soils and stabilized soils (Ghorbani and Hasanzadehshooiili 2018, Mozumder and Laskar 2015, Saadat and Bayat 2022, Sihag *et al.* 2019), geotechnical characteristics of oil contaminated sandy soils or sediments (Alidoosti *et al*. 2016; Hajian and Ghane 2015), rock engineering classification system (Jalalifar *et al.* 2011), pile bearing capacity, settlement and swell (Luat *et al.* 2020, Pooya Nejad *et al.* 2009, Sivapullaiah *et al*. 2009) and thermo-hydro-mechanical coupling behavior (Kwon and Lee 2018).

Despite the mentioned research efforts, there is a lack of comparative studies regarding the use of ANN and ANFIS to predict the G_{max} of granular material. In the current study, both ANN and ANFIS are applied to estimate the G_{max} of granular soils, in order to compare the results with a common classical model-based method a modified empirical equation is proposed based on the lab results.

2. Materials and experimental methods

In this study, consolidation stress ratio (the ratio of horizontal stress to vertical stress), mean effective confining stress, void ratio, gravel content and depositional method were selected as the controlled variables to design a suitable experimental configuration. The summary of the tests, performed on reconstituted granular specimens, is listed in Table 1. As it is depicted in Fig. 1, the tests were conducted by RC and BE devices. The first group of tests was conducted to study the effect of mean effective stress, gravel content and relative density on the G_{max}. In previous studies, the resonant column has been used to validate the results of bender element tests (Camacho-Tauta *et al.* 2011, Camacho-tauta *et al.* 2013, Ferreira *et al*. 2007, Hoyos *et al.* 2015, Youn *et al*. 2008). In this study, the purpose of the column tests was to validate the results of the element tests. As shown from Table 1, a number of specimens were randomly selected to evaluate BE results by comparing them to RC results. Groups-2(a) and 2(b) were conducted to study the effect stress ratio on the G_{max} of specimens containing various gravel contents under constant confining effective stress (σ'_3 100, 300 or 600 kPa). Group-2(c) was conducted to study the effect stress ratio on the G_{max} of specimens containing various gravel contents under constant mean effective stress (σ'_m = 300 kPa). Group-3 was conducted to study the effect depositional method (WP, AP and WT) on the G_{max}. It is noteworthy that in this study, all specimens were saturated before testing that the initial moisture content of the samples did not affect the results. In other words, the only effective factor on the results was the different fabric created by the sample preparation methods. A pair of BEs which was installed on the top cap and base pedestal of the triaxial apparatus was used to measure the G_{max}, totally it was designed so that it could be able to work under both isotropic and anisotropic conditions. More details about test procedures can be found in Bayat and Ghalandarzadeh (2020). Various interpretation techniques, including the start–to-start technique, the peak–to-peak technique, the cross correlation and the cross power techniques, have been proposed to determine the travel time (Gu *et al.* 2015). Note that in this research, the first arrival detection was used to provide the travel time estimations (see Fig. 2). Therefore, knowing that the distance of travel is the tip-to-tip distance between source and receiver, the speed of the shear wave, *Vs*, can be determined. In the current study, a single sinusoidal pulse having a frequency of 6-25 kHz was used as the transmitted signal. The results of BE tests show that the desired frequencies range depended on the gravel content. In general, the desired frequencies range increased with the increasing gravel content. Outside of these the desired frequencies range, very noisy received signals were found to be produced. The resonant frequency of the bender element is a very important parameter for near-field effect and travel time determinations.

Fig. 1 (a) Resonant column device (b) Bender element setup used for the current study

Various interpretation techniques, including the start–to-start technique, the peak–to-peak technique, the cross correlation and the cross power techniques, have been proposed to determine the travel time (Gu *et a*l. 2015). Note that in this research, the first arrival detection was used to provide the travel time estimations (see Fig. 2). Therefore, knowing that the distance of travel is the tip-to-tip distance between source and receiver, the speed of the shear wave, *Vs*, can be determined. In the current study, a single sinusoidal pulse having a frequency of 6-25 kHz was used as the transmitted signal. The results of BE tests show that the desired frequencies range depended on the gravel content. In general, the desired frequencies range increased with the increasing gravel content. Outside of these the desired frequencies range, very noisy received signals were found to be produced. The resonant frequency of the bender element is a very important parameter for near-field effect and travel time determinations.

As it is illustrated in Fig. 2, the arrival point of the S-wave front can be masked by the faster-travelling P-wave near-field component which is called the near-field effect. In the first arrival, travel time of the signal refers to the time between the start of the transmitted wave and the start of the receiver wave by ignoring the initial weak signal or near-field effect. In this study, a free-free RC apparatus was used to validate the interpretation methods used for BE testing.

Table 1 Summary of the tests details

Test Group	σ'_3 (*Kpa*)	*GC (%)*	*Dr (%)*	*Kc*	*specimen preparation technique* ††	*No. of tests*
Group-1	30 50 75 100 150 200 300 400 500 600	0 30 50 75	10 30 60	1	WT	120 BE; 31 RC
Group-2(a)	300	0 30 50 75	60	0.5 0.75 1 1.25 1.5	WT	20 BE
Group-2(b)	100 600	0 30 50 75	60	0.5 1 1.5	WT	24 BE
Group-2(c)	300	0	60	0.5 0.75 1 1.25 1.5	WT	5 BE
Group-3	100 300 600	0 50	10 60	1	WT AP WP	24 BE

As it is shown in Table 1, the RC test was conducted on some specimens and the results were compared with those of the BE results, which is known as a very accurate dynamic test (Gu *et al.* 2015). Reference to Fig. 3, the G_{max} values obtained through both techniques (i.e., BE and RC) are in acceptable agreement; however, G_{max} values obtained by BE technique for the specimens containing 75% gravel were consistently lower than the corresponding values of G_{max} obtained by RC. The G_{max} of the specimens with gravel contents of less than 75% from both methods (BE and RC) were in good agreement. This indicates that the BE test does not perform well in uniform coarse-grained soils. It can be conducted that the particle size of granular soils has an important effect on the shape of the received signals.

In this study, ,the ratio of horizontal stress to vertical stress in consolidation stage namely the "consolidation stress ratio (*Kc*)", was used to describe induced anisotropic consolidation (Bayat and Ghalandarzadeh 2020). *Kc* is defined as a physical property due exclusively to the strain associated with applied stress. In the current study, the consolidation stress ratio was used to describe anisotropic stress condition as

$$Kc = \frac{\sigma'_h}{\sigma'_v} \tag{2}$$

where σ'_h and σ'_v are horizontal and vertical effective stress, respectively.

Cylindrical specimens with a diameter of 100 mm and a height of 200 mm were prepared by either wet tamping (WT), water pluviation (WP) or air pluviation (AP) technique. As depicted in Fig. 4, four gradations of granular material were used to study the influence of grading characteristics on the G_{max}.

3. Neural Network (NN)

3.1 Artificial Neural Network (ANN)

ANN is a simplified model of mammal neurons as especially the human brain's neuron-based architecture. The main feature of neuron is its ability to learn from data. The neurons are connected to other neurons in a network style

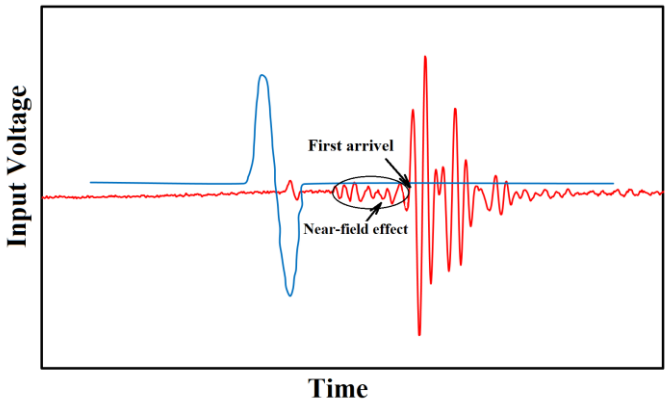

Fig. 2 BE input and output signals

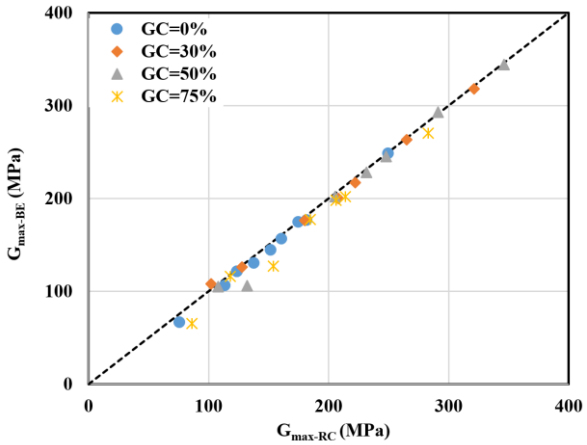

Fig. 3 Comparison between BE and RC results

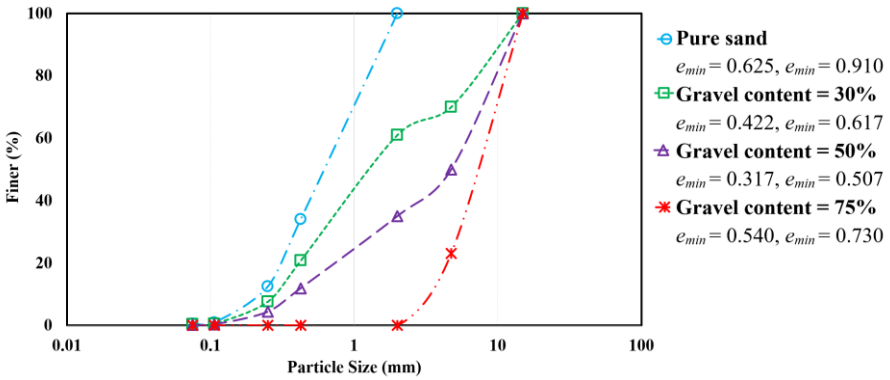

Fig. 4 Grain size distribution curves of the granular soil mixtures.

so that the brain has a strong connection of neurons. Each of the inputs of a neuron is entering via synapses and takes a separate coefficient namely “weight” (Fig. 5(a)). The neuron first summing the weighted inputs and then a threshold function is activated namely “activation function” (Fig. 5(a)) the output of this function is the final output of the neuron. Based on this natural behavior of neuron the mathematical model of a neuron is as shown in Fig. 5(b).

Generally, there are two categories of artificial neural networks: supervised and up-supervised, the first category as its name shows is the neural networks which has a trainer and consequently are trained by a set of the experimental data (or on the other hand known pairs of {inputs, outputs}). The second category works without training i.e. Hopfield neural networks are unsupervised. As the details of this topic are beyond the scope of this article, for more details readers can read chapter one in the book written; on this topic; by Hajian and Styles (2018). Among various kinds of supervised neural networks one of the most common used, especially in engineering problems, is MLP. MLP includes input layer, hidden/s layer/s and output layer; each of the layers has a number of neurons and each neuron of a layer is connected directly to all neurons of the next layer (unless output layer that has no layer after) with a

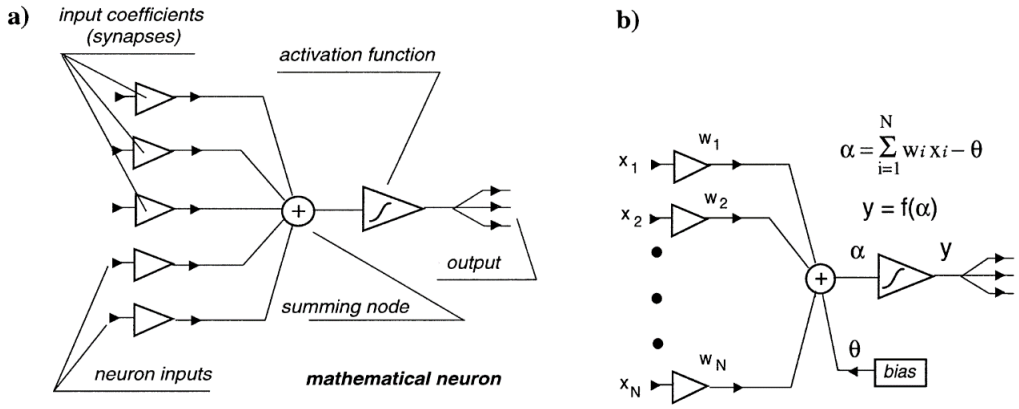

Fig. 5 (a) Mathematical model of a 'neuron'and (b) the weighted sum of the inputs is rescaled by an activation function (redrawn after Hajian and Styles 2018)

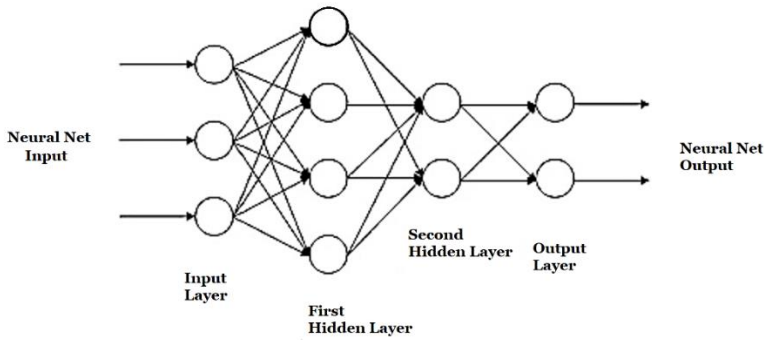

Fig. 6 Schematic of an MLP with three inputs, 4 and 2 neurons in the first and second hidden layer; respectively and two outputs; we show this architecture by MLP (3, 4, 2, 2)

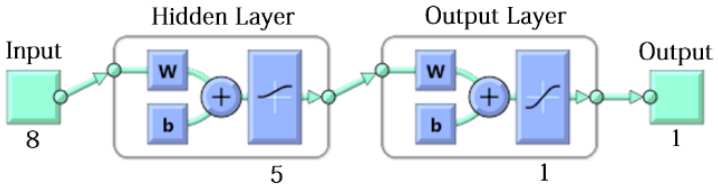

Fig. 7 Architecture of the MLP (8,5,1); found as suitable MLP to estimate G_{max}

weighted connection(see Fig. 6).Training of an MLP means to find the weights which best image known inputs to known outputs with minimum error (difference between target output and estimated output can be measured by statistical error indexes i.e. Absolute error, relative error, MSE: Mean Square Error or RMSE: Root Mean Square Error, etc.).

To determine the number of the hidden layers and the number of neurons in the hidden layers there is no clear formula and they are usually determined through testing different values i.e., by trial and error. Although for problems with higher degree of complexity and nonlinearity (which needs to a large amount of training data) usually two hidden layers are tested but for other problems with low or medium level of complexity and/or nonlinearity only one hidden layer is enough. In this study we found an MLP with one hidden layer is enough and the optimum number of neurons in the hidden layer was determined by testing from initial N_{int}=1 to final N_{fin}=10, described with more details in the next section.

3.2 Design and test of MLP to estimate G_{max}

To find a suitable architecture of Multi-Layer Perceptron neural network to estimate G_{max}, different MLPs with different number of hidden layers and different number of neurons in the hidden/s layer were tested (Fig. 8), also for each architecture different learning algorithms were tested and their RMSE and R^2 as indexes of the performance were calculated and compared. Finally, the MLP (8,5,1), with detailed specifications mentioned in Table 2 and Fig. 7 was selected as optimized architecture to estimate G_{max} with less RMSE and highest R^2.

4. ANFIS

4.1 Principles of ANFIS

ANFIS approximates the functional relations between responses and input variables of the process under study by

Table 2 Specifications of MLP designed to estimate G_{max} of granular soil

Parameter	Value
Number of inputs	Equal to number of selected geotechnical parameters of granular soil: 8
Number of outputs	1
Number of hidden neurons(M)	Calculated adaptively
Activation function of hidden layer neurons	Sigmoid
Activation function of output layer neurons	Sigmoid
Training Algorithm	Levenberg- Marquardt
Maximum number of hidden neurons to test	From 1 to 10 (Finally we found N=5 is the optimized, see Fig. 8)
Maximum number of epochs	1000

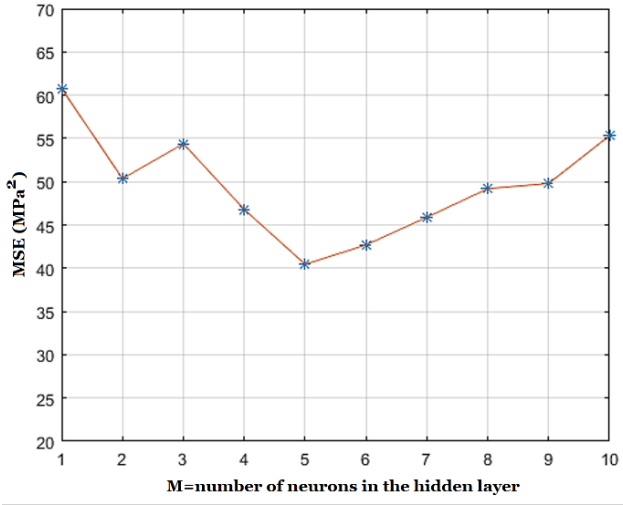

Fig. 8 Mean Square Error (MSE) versus number of neurons in the hidden layer of (8, M, 1) MLP model, as it can be seen the minimum MSE is for M=5

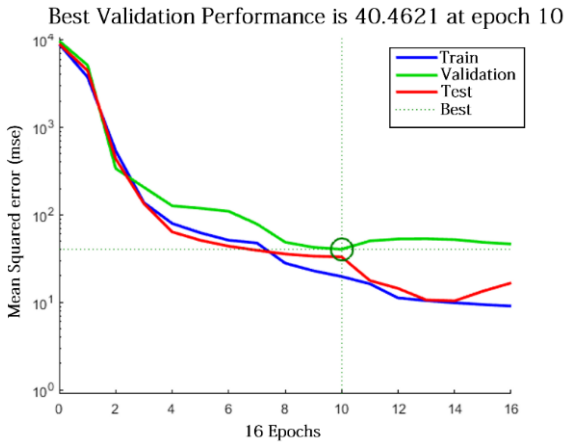

Fig. 9 MLP (8, 5, 1) neural network training performance; MSE of MLP for train, validation and test data

gradually fine-tuning the values of parameters. The ANFIS architecture is shown in Fig. 11. The circular nodes are fixed whereas the square nodes have parameters to be learnt. Two Rules Sugeno ANFIS has rules of the form

$$\begin{aligned} &If\ x\ is\ A_1\ and\ y\ is\ B_1 \quad THEN\ f_1 = p_1x + q_1y + r_1 \\ &If\ x\ is\ A_2\ and\ y\ is\ B_2 \quad THEN\ f_2 = p_2x + q_2y + r_2 \end{aligned} \tag{3}$$

For training the network, there is a forward pass which propagates the input vector through the network layer by layer and in the backward pass, the error is sent back through the network in a similar manner to back propagation.

Layer 1: The output of each node is

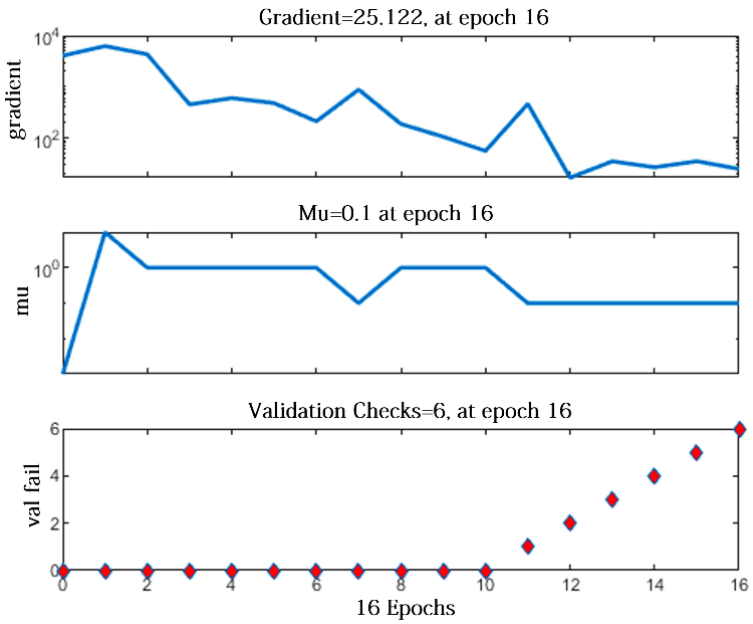

Fig. 10 Gradient, Momentum and validation checks versus epoch number for MLP (8,5,1) training

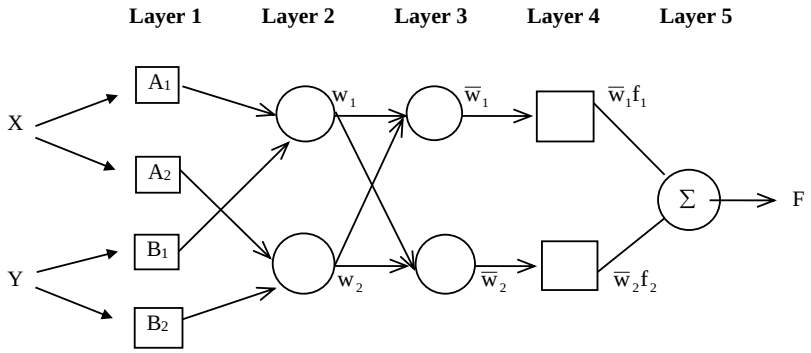

Fig. 11 ANFIS architecture for a two rule Sugeno system

$$O_{1,i} = \mu_{A_i}(x) \qquad for\ i = 1,2$$
$$O_{1,i} = \mu_{B_{i-2}}(y) \qquad for\ i = 3,4 \tag{4}$$

So, $Q_{1,i}(x)$ is essentially the membership grade for x and y. The membership functions can be anything but we used the bell shaped function given by

$$\mu_A(x) = \frac{1}{1 + \left|\frac{x - c_i}{a_i}\right|^{2b_i}} \tag{5}$$

where a_i, b_i, c_i are parameters to be learnt. These are the premise parameters.

Layer 2: Every node in this layer is fixed. This is where the t-norm is used to 'AND' the membership grades - for example the product

$$O_{2,i} = w_i = \mu_{Ai}(x)\mu_{Bi}(y), \qquad i = 1,2 \tag{6}$$

Layer 3: Layer 3 contains fixed nodes which calculate the ratio of the firing strengths of the rules

$$O_{3,i} = \overline{w}_i = \frac{w_i}{w_1 + w_2} \tag{7}$$

Layer 4: The nodes in this layer are adaptive and perform the consequences of the rules

$$O_{4,i} = \overline{w}_i f_i = \overline{w}_i(p_i x + q_i y + r_i) \tag{8}$$

The parameters to be determined in this layer (p_i, q_i, r_i) are referred to as the consequent parameters.

Layer 5: There is a single node here that computes the overall output

$$O_{5,i} = \sum_i \overline{w}_i f_i = \frac{\sum_i w_i f_i}{\sum_i w_i} \tag{9}$$

This then is typically how the input vector is fed through the network layer by layer. There are several approaches for training but in this study we used the hybrid learning algorithm proposed by Jang *et al.* (1997) which is a combination of Steepest Descent and Least Squares Estimation (LSE).

methods, respectively.

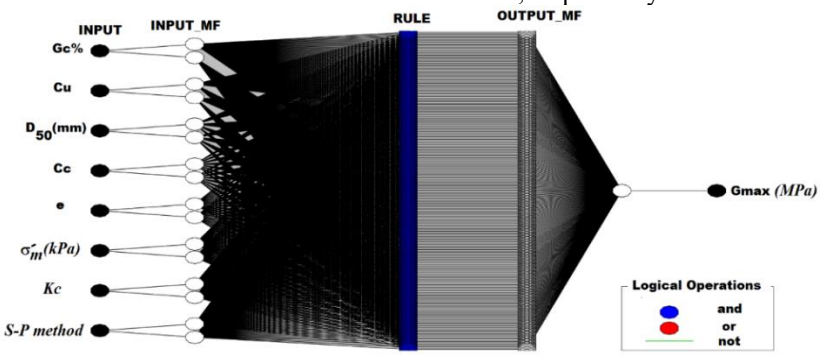

Fig. 12 The ANFIS structure of the layers, nodes and connections designed to estimate Gmax

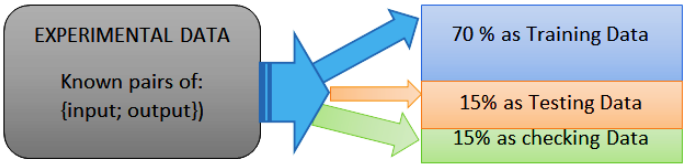

Fig. 13 Division of experimental data into groups of training, testing and checking sets

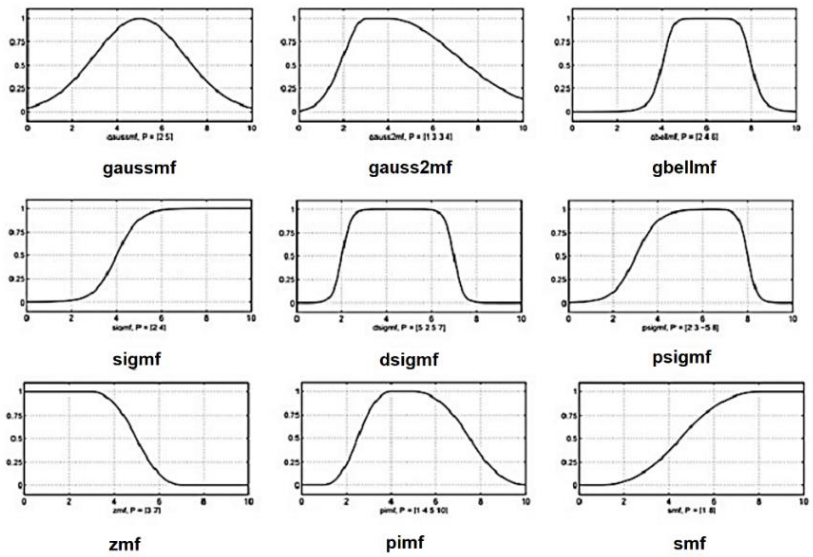

Fig. 14 Different types of MF's for inputs of ANFIS; generaly to select the optimized structure of ANFIS (Hajian and Styles 2018)

4.2 Architecture of ANFIS for estimating G_{max}

To design and test of ANFIS for estimating G_{max} of the granular soil, the steps mentioned below were followed (in order of the numbers):

Step 1: Selecting suitable inputs as shown in Fig. 12. In this figure, gravel content (GC), uniformity coefficient (C_u), average particle size (D_{50}), coefficient of curvature(C_c), void ratio (e), mean effective confining pressure (σ'_m), anisotropic consolidation ratio (K_c), and specimen preparation method (*S-P method*) were regarded as input variables of Artificial Neural Networks and ANFIS. Note that *S-P method* coefficient is dependent on specimen preparation method and in the current study, it is considered as a constant equal to 1, 1.1 and 1.2 for WP, AP and WT

Step 2. Normalization of experimental data pairs (known {inputs, output}) using Eqs. (9) and (10)

$$normalized(input)=(input-input_{min})/(input_{max}-input_{min}) \quad (10)$$

$$normalized(output)=(output-output_{min})/(output_{max}-ouput_{min}) \quad (11)$$

Step 3. Division of data into three groups: training data (70% of Total number of Experimental Data: TED), testing data (15% of TED), checking data (15% of TED) as shown in Fig. 13. The role of testing and checking data in training process of an ANFIS is as the same as the role of testing and validation data in training of an MLP. The ANFIS training criteria is stopped when the MSE for checking data is increasing while it is decreasing for both testing and training data. In this study, as the total number of

Table 3 Information of ANFIS models

Option	model#A	model#B
Number of nodes	555	
Number of linear parameters	256	2304
Number of nonlinear parameters	32	48
Total number of parameters	288	2352
Number of training data pairs	131	
Number of testing data pairs	28	
Number of checking data pairs	28	
Number of fuzzy rules	256	
Minimal training RMSE	13.482140	2. 010016

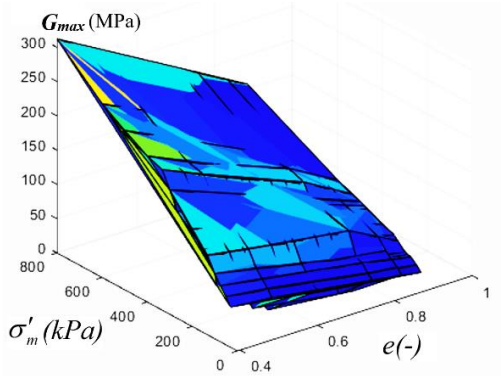

Fig. 17 Effects of void ratio and mean effective confining pressure on G_{max}

experimental data pairs; measured in the lab; were 187 the training, testing and validation data sets contains 131, 28, 28 pairs, respectively.

Step5: Selecting the optimization method to train ANFIS with training data: back propagation or hybrid; in this study we found hybrid as more suitable training algorithm.

Step6: selecting number of epochs for training stop criteria; in this study we found 40 epochs is enough (because after this epoch the value of MSE was fixed).

Step7: calculating the MSE and R^2 and playing with number of MF's, type of MF's for inputs and type of MF for output until getting to desired values of MSE and R^2.

As it was described in the steps of designing of ANFIS, in order to find a suitable architecture of ANFIS for our study, we tested various ANFISs' with different number and type of Membership functions for input and different types of MFs' for output (linear or constant). The results were compared by their RMSE and R^2 and finally we found that the ANFIS model#B with [2 2 2 2 2 2 2 2] triangle membership functions reach to minimum RMSE and maximum R^2 for estimation of G_{max}. As some examples the RMSE for ANFIS [2 2 2 2 2 2 2 2] with Gaussian (ANFIS model#A) and triangle MF's (ANFIS model#B) is illustrated in Figs. 15 and 16, respectively. The information of ANFIS model#A, model#B is given in Table 3.

5. Results and discussion

The G_{max} values were determined from BE testing. Based on the results, the void ratio, mean effective confining pressure, gravel content, anisotropic consolidation and initial fabric anisotropy produced during specimen preparation on the G_{max} values were assessed.

5.1 Laboratory tests results

To get a better understanding about the effects of each couple of inputs on G_{max}, the data were interpolated for each couple of inputs as

$$G_{max}^{interpolated} = \text{interpolation of } ((G_{max}), (X_i, X_j)) \quad i \neq j,\ i=1,2,\ldots 8,\ j=1,2,..,8 \tag{10}$$

where X_i and X_j are i^{th} and j^{th} experimental input vector, respectively, and G_{max} is the vector of experimental data. Note that (X_i, X_j) and (X_j, X_i) are accounted as only one pairs because the 3D plot of $((G_{max}), (X_i, X_j))$ is the same as 3D plot of $((G_{max}), (X_j, Xi))$ with a different view angle.

After interpolating, G_{max} was plotted versus all pairs of (x_i, x_j),as we have 8 variables as input $\binom{8}{2} = 28$ plots were provided, in this section some of important plots are presented and interpreted, as samples.

Effect of void ratio and mean effective confining pressure on G_{max} of the specimens are shown in Fig. 17 As shown, decreasing void ratio or increasing mean effective confining pressure results in increasing G_{max} which is in good agreement with previous studies (Rahman *et al*. 2012, Ueno *et al.* 2019, Wang and Kuwano 1999, Yamada *et al*. 2008).

Fig. 18 shows the effect of depositional methods on G_{max} of the specimens with various gravel content. For a given depositional method, G_{max} increases nonlinearly with an increase in gravel content up to 50% and then decreased. Also the results indicate that G_{max} of the specimen prepared with the WT and WS techniques recorded the highest and lowest values, respectively which were also in agreement with previous finding (Rashidian *et al*. 1995, Gu *et al.* 2015). The results indicate that G_{max} increased with an increase in GC up to 50% and then decreases with increasing gravel content. The specimen with GC=50% recorded the highest G_{max} at a given σ'_m and e. Note that the specimens containing 50% gravel had the lowest void ratio when compared to other specimens at a given relative density. The values of e_{max} and e_{min} have been shown in Fig. 4. As shown, the values of e_{max} and e_{min} decreased significantly when the gravel content increased from 0 to 50%. For gravel contents of 0 to 50%, the void between the particles decreased and the gravel particles float in the sand matrix. The sample containing 50% gravel has the lowest void between the particles for a given relative density. The values of e_{max} and e_{min} increased as the gravel content increased from 50% to 75% and the void between the particles increased. As shown from Fig. 4, the values for e_{max} and e_{min} increase with an increase in gravel content to 50%, at which point contact between the gravel grains increases.

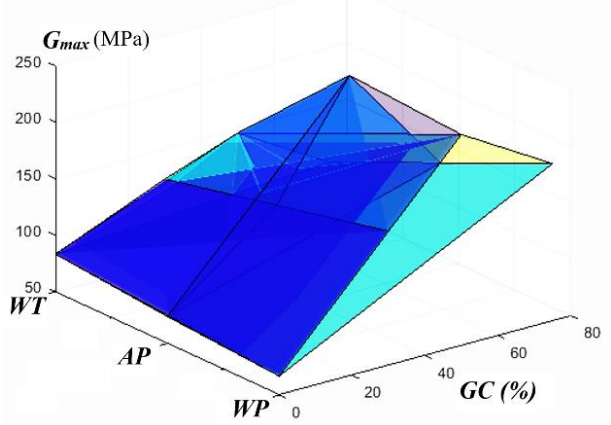

Fig. 18 Effects of specimen preparation method and gravel content on G_{max}

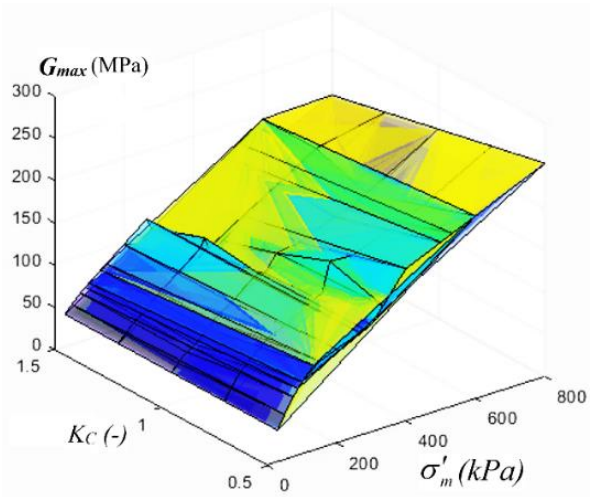

Fig. 19 Effects of consolidation stress ratio and mean effective confining pressure on G_{max}

Fig. 19 shows the effect of anisotropic consolidation ratio on G_{max} of the specimens tested under various mean effective confining pressures. As shown, a decrease in anisotropic consolidation ratio increased G_{max} at a given mean effective confining pressure; this could be the result of an increase in effective stress in the direction of wave propagation which is the vertical direction.

5.2 A new empirical equation for prediction of G_{max}

Based on the BE results, a general equation is presented as follows that can be used to predict the G_{max} of granular soils

$$G_{\max} = A_{sp} \times \left[\frac{(3.02-e)^2}{(0.72+e)}\right] \times (\sigma'_m)^{0.59} \times (1+K_C)^{-0.41} \quad (13)$$

where G_{max} denotes the maximum shear wave velocity (MPa), e denotes the void ratio, σ'_m denotes the mean effective confining pressure (kPa) and K_c denotes the consolidation stress ratio ($K_c=\sigma_h/\sigma_v$). A_{sp} is a model parameter reflecting the fabric dependence of the soil, which is primarily affected by the deposition technique in the current study. The values of A_{sp} and other constants were calculated using nonlinear least squares analysis and determined such that the sum of squares of the difference between the predicted G_{max} value and the corresponding measured value of G_{max} could be minimized.

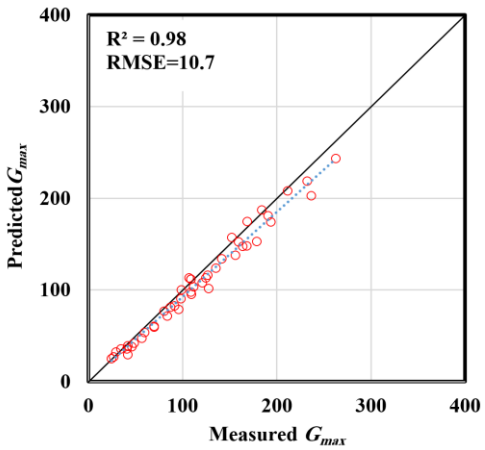

Fig. 20 G_{max}-values predicted by Eq. (13) versus measured G_{max}-values in the current study

It's necessary to mention that only 70 percent of experimental data was used for training and the remained fraction of data was used for validation. Using the nonlinear least squares analysis, the values of parameter A_{sp} were 1.2, 1.1 and 1 for the specimens prepared by the WT, AP and WP techniques, respectively as well as MLP and ANFIS models. The results of the tests indicated that the WT and WP specimens exhibited the highest and lowest values of G_{max}, respectively. The G_{max} values of the WT specimens were approximately 11-43% higher than those of the WS specimens, but the G_{max} values of the AP specimens were about 3–19% higher than those of the WS specimens. The results show that the difference in the soil fabric introduced by the different specimen preparation techniques (WT, AP and WP) have an important influence on the G_{max}. Yang *et al.* (2008) compared the fabric anisotropy of granular soil samples prepared by different sample preparation techniques. They stated that the sample prepared by the AP technique was more anisotropic in its fabric, and the preferential contact of granular particles is vertical. In contrast, sand sample prepared by the WT technique was more isotropic in their fabric.

In order to validate the applicability of the proposed equation (Eq. (13)), the measured G_{max} is compared with that predicted G_{max} for all specimens (see Fig. 20). As shown, the value of R^2 and RMSE between the measured and predicted values are 0.98034 and 10.70712, respectively. This appears to be the result of using the proposed equation to predict the G_{max} of the granular soils easily and precisely.

5.3 Modelling results

Fig. 21 shows a comparison between measured values of G_{max} and predicted ones using ANN model. Comparing of the R^2 and RMSE values for each of the models, used in this

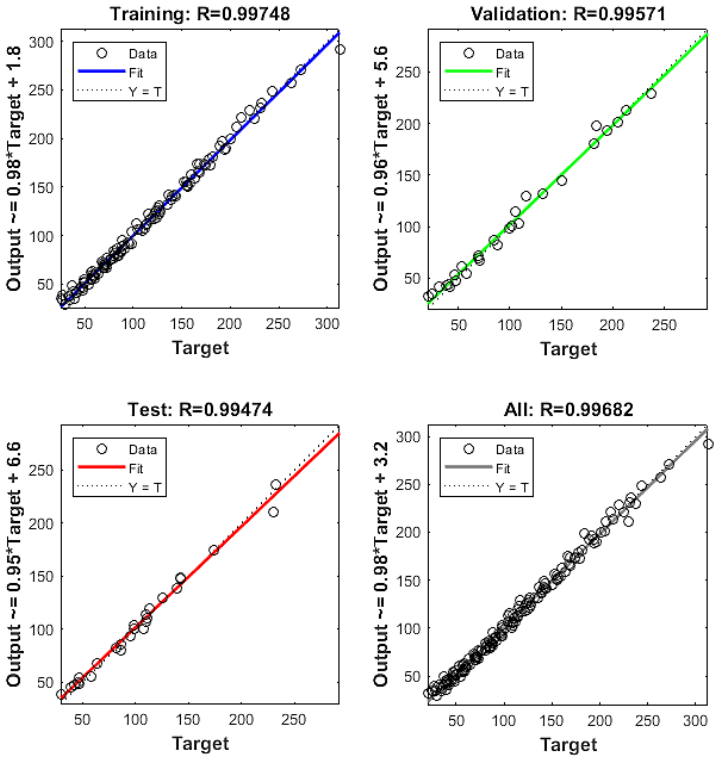

Fig. 21 Regression of output-target (estimated G_{max} versus measured G_{max}) for MLP (8,5,1) with 1 hidden layer and 5 neurons in this layer, for training, testing, validation

Table 4. Values of RMSE and R^2 between observed and predicted G_{max} for the empirical, MLP and ANFIS models

Methodology	R^2	RMSE (MPa)	Running time (min) †
Empirical model (Eq. (13))	0.98201	11.53420	0.9 min
MLP	0.99682	6.308980	1.6 min
ANFIS	0.98767	2.010016	5.4 min

†The running time, for ANN and ANFIS, means the total time elapsed for training and calculating final output

research, is presented in Table 4. The results show that the R^2 value for all empirical, ANN and ANFIS models are very close (near to 0.99) but the RMSE value is different so that ANFIS model has the minimum value of this type of error. Also between MLP and Empirical model, from the view angle of RMSE; MLP is so better, because MLP's RMSE is about half of that for Empirical. Another advantage of both models ANN and ANFIS is that when they are trained for a domain of inputs, they work as well for any data set belongs to this domain. Consequently, it's not necessary to repeat the whole computations for a new training process. However, training of an ANFIS or ANN for a domain of inputs, at the first stage, needs more time than Empirical model because there are more parameters to calculate like weights of each of the neurons, activation functions for ANN and membership functions (types and number) of input, output and if-then fuzzy-rules. As it is shown in Table 4, there is a trade-off between the elapsed time of running codes and the accuracy of the methods, while the time needs for running ANFIS codes is the maximum, its RMSE error is the minimum (showing its higher accuracy).

6. Conclusions

In order to investigate the effect of grading characteristics, void ratio, mean effective confining stress, consolidation stress ratio and fabric anisotropic on the G_{max} of granular soils, a series of BE tests was carried out on fully saturated specimens. Based on the results, an empirical model was developed for prediction of G_{max}. The artificial neural network (ANN) and Adaptive Neuro Fuzzy Inference System (ANFIS) models were also selected as estimation models to predict the G_{max} values. The results of empirical model (Eq. (13)), which is a model-based technique, was compared to data-based methods ANN and ANFIS. Based on the results of the tests and performed analysis, the following conclusions can be drawn:

The results of the BE tests show that G_{max} rise up with an increase in gravel content up to 50% and then decreases with increasing gravel content. The specimen with gravel content equal to 50% recorded the highest G_{max}. on the other hand, the increasing σ'_m or decreasing e result in a nonlinear increase in G_{max}. The results of the tests under anisotropic consolidation indicate that increasing of K_c leads to decreasing G_{max}. The results of the tests also show that depositional method has an important effect on the G_{max}. The G_{max} reaches its highest or lowest value for the specimen prepared using the WT and WP techniques, respectively.

Model based is the methodology that tries to fit data into a pre-assumed equation with unknown coefficients and/or parameters and is generally a type of regression while data-based methods don't assume any equation of the model and

try to learn the output trend from experimental data. To evaluate the method accuracy, efficiency and speed of the methods, RMSE, R^2 and running time of each model was calculated.

The evaluations showed that both data-based methods, ANN and ANFIS, have much lower RMSE values or in the other hand higher accuracy than that of Empirical method while having very close values of R^2 shows their similar efficiency. Also among all, ANFIS has the minimum RMSE that shows the best accuracy among the investigated models. Furthermore, the elapsed time to run the models, to estimate G_{max}, was compared. The results show that ANFIS takes the maximum time, the main reason is basically for its bigger structure which needs more computations for determination of both the membership functions and if-then fuzzy rules. Thinking through a framework of Trade-Off philosophy, this additional time is the cost that ANFIS pays to get the maximum accuracy compared to ANN and empirical methods. However, it's necessary to mention that one-time that ANFIS is trained suitably for a domain, it works as well for any inputs belongs to the training domain and so the elapsed time decreased as the training process is not necessary to be repeated. The power of ANFIS for estimating G_{max} with RMSE less than 2MPa assures the experts to use it t as a useful technique to predict the laboratory results without needing to pay any more to do more experiments, when there is enough experimental data set.

References

Alidoosti, A., Ajalloian, R. and Alireza, H. (2016), "Assessment of Geotechnical properties of sediments along Isfahan Line2 subway with emphasis on in-situ tests", *Proceedings of the 5th International conference on Geotechnical Engineering and Soil Mechanics, Tehran, Iran*.

Bayat, M. and Ghalandarzadeh, A. (2018), "Stiffness degradation and damping ratio of sand-gravel mixtures under saturated state", *Int. J. Civil Eng.*, **16**(10), 1261-1277. https://doi.org/10.1007/s40999-017-0274-8.

Bayat, M. and Ghalandarzadeh, A. (2019), "Influence of depositional method on dynamic properties of granular soil", *Int. J. Civil Eng.*, **17**(6), 907-920. https://doi.org/10.1007/s40999-019-00412-7.

Bayat, M. and Ghalandarzadeh, A. (2020), "Modified models for predicting dynamic properties of granular soil under anisotropic consolidation", *Int. J. Geomech.*, **20**(3), 04019197. https://doi.org/10.1061/(asce)gm.1943-5622.0001607.

Bosiljkov, V.Z., Totoev, Y.Z. and Nichols, J.M. (2005), "Shear modulus and stiffness of brickwork masonry: An experimental perspective", *Struct. Eng. Mech.*, **20**(1), 21-43. https://doi.org/10.12989/sem.2005.20.1.021.

Camacho-Tauta, J., Cascante, G., Santos, J.A., Viana da Fonseca, A.A. and Dos Santos, J.A. (2011), "Measurements of shear wave velocity by resonant-column test, bender element test and miniature accelerometers", *Proceedings of the 2011 Pan-Am Geotechnical Conference*, (1998), 1-9. https://www.academia.edu/download/45552620/Measurements_of_shear_wave_velocity_by_r20160511-16261-1xq5sit.pdf. Accessed 18 May 2020.

Camacho-tauta, J.F., David, J. and Álvarez, J. (2013), "Comparison between resonant-column and bender element tests on three types of soils", *Comparison between resonant-column and bender element tests on three types of soils*, **80**(1), 163-172. http://www.scielo.org.co/pdf/dyna/v80n182/v80n182a20.pdf

Carette, J. and Staquet, S. (2016), "Monitoring the setting process of eco-binders by ultrasonic P-wave and S-wave transmission velocity measurement: Mortar vs concrete", *Constr. Build. Mate.*, **110**, 32-41. https://doi.org/10.1016/j.conbuildmat.2016.02.019.

Cha, M. and Cho, G.C. (2007), "Shear strength estimation of sandy soils using shear wave velocity", *Geotech. Test. J.*, **30**(6), 484-495. https://doi.org/10.1520/gtj100011.

Chang, I. and Cho, G.C. (2010), "A new alternative for estimation of geotechnical engineering parameters in reclaimed clays by using shear wave velocity", *Geotech. Test. J.*, **33**(3). https://doi.org/10.1520/GTJ102360.

Cho, H.I., Sun, C.G., Kim, J.H. and Kim, D.S. (2018), "OCR evaluation of cohesionless soil in centrifuge model using shear wave velocity", *Geomech. Eng.*, **15**(4), 987-995. https://doi.org/10.12989/gae.2018.15.4.987.

Clayton, C.R.I. (2011), "Stiffness at small strain: Research and practice", *Geotechnique*, **61**(1), 5-37. https://doi.org/10.1680/geot.2011.61.1.5.

Dyvik, R. and Madshus, C. (1986), "Lab measurements of Gmax using bender elements", In *Publikasjon - Norges Geotekniske Institutt*. https://doi.org/10.1016/0148-9062(87)92023-7.

El Mosallamy, M., El Fattah, T.T.A. and El Khouly, M. (2016), "Experimental study on the determination of small strain-shear modulus of loess soil", *HBRC J.*, **12**(2), 181-190. https://doi.org/10.1016/j.hbrcj.2014.11.010.

Ferreira, C., da Fonseca, A. and Santos, J.A. (2007), "Comparison of simultaneous bender elements and resonant", *Soil Stress-Strain Behavior: Measurement, Modeling and Analysis. Solid Mechanics and Its Applications*, 523-535.

Ghorbani, A. and Hasanzadehshooiili, H. (2018), "Prediction of UCS and CBR of microsilica-lime stabilized sulfate silty sand using ANN and EPR models; application to the deep soil mixing", *Soils Found.*, **58**(1), 34-49. https://doi.org/10.1016/j.sandf.2017.11.002.

Goudarzy, M., Rahemi, N., Rahman, M.M. and Schanz, T. (2017), "Predicting the maximum shear modulus of sands containing nonplastic fines", *J. Geotech. Geoenviron. Eng.*, **143**(9), 06017013. https://doi.org/10.1061/(asce)gt.1943-5606.0001760.

Gu, X., Yang, J. and Huang, M. (2013), "Laboratory measurements of small strain properties of dry sands by bender element", *Soils Found.*, **53**(5), 735-745. https://doi.org/10.1016/j.sandf.2013.08.011.

Gu, X., Yang, J., Huang, M. and Gao, G. (2015), "Bender element tests in dry and saturated sand: Signal interpretation and result comparison", *Soils Found.*, **55**(5), 951-962. https://doi.org/10.1016/j.sandf.2015.09.002.

Hajian, A. and Ghane, A. (2015), "Prediction of Geotechnical Behavior (Shear Strength, Compression, Friction Angle) of Oil Contaminated Sandy Soils using Artificial Neural Networks", In *3th international conference on Oil, Gas and Petrochemical , Shahid Behesti University, Tehran, Iran*.

Hajian, A. and Styles, P. (2018), *Application of Soft Computing and Intelligent Methods in Geophysics*. Cham: Springer International Publishing. https://doi.org/10.1007/978-3-319-66532-0.

Hardin, B.O. and Black, W.L. (1967). "Sand stiffness under various triaxial stresses", *J. Terramech.*, **4**(3), 70.

https://doi.org/10.1016/0022-4898(67)90133-4.

Hardin, B. and Richart, F. (1963), "Elastic wave velocities in granularsoils", *J. Soil Mech. Found. Div.*, **89**(1), 33-66.

Hoyos, L.R., Suescún-Florez, E.A. and Puppala, A.J. (2015),. "Stiffness of intermediate unsaturated soil from simultaneous suction-controlled resonant column and bender element testing", *Eng. Geol.*, **188**, 10–28. https://doi.org/10.1016/j.enggeo.2015.01.014.

Hussien, M.N. andKarray, M. (2016), "Shear wave velocity as a geotechnical parameter: An overview", *Can. Geotech. J.*, **53**(2), 252-272. https://doi.org/10.1139/cgj-2014-0524.

Jalalifar, H., Mojedifar, S., Sahebi, A.A. and Nezamabadi-pour, H. (2011), "Application of the adaptive neuro-fuzzy inference system for prediction of a rock engineering classification system", *Comput. Geotech.*, **38**(6), 783-790. https://doi.org/10.1016/j.compgeo.2011.04.005.

Jang, J.S.R., Sun, C.T. and Mizutani, E. (2005), *Neuro-Fuzzy and Soft Computing-A Computational Approach to Learning and Machine Intelligence [Book Review]. IEEE Transactions on Automatic Control*, 42. https://doi.org/10.1109/tac.1997.633847

Kwon, S. and Lee, C. (2018), "Thm analysis for an in situ experiment using FLAC3D-TOUGH2 and an artificial neural network", *Geomech. Eng.*, **16**(4), 363-373. https://doi.org/10.12989/gae.2018.16.4.363.

Li, B. (2011), "Effect of fabric anisotropy on the dynamic mechanical behavior of granular materials", *Techniques*. http://etd.ohiolink.edu/send-pdf.cgi/Li Bo.pdf?case1291071699

Li, Y. (2016), "Teaching programming based on computational thinking", *Proceedings - Frontiers in Education Conference, FIE*, *2016-Novem*(96), 241. https://doi.org/10.1109/FIE.2016.7757408.

Liang, J., Han, B., Todorovska, M.I. and Trifunac, M.D. (2018), "2D dynamic structure-soil-structure interaction for twin buildings in layered half-space II: Incident SV-waves", *Soil Dyn. Earthq. Eng.*, **113**, 356-390. https://doi.org/10.1016/j.soildyn.2018.05.023.

Luat, N.V., Lee, K. and Thai, D.K. (2020), "Application of artificial neural networks in settlement prediction of shallow foundations on sandy soils", *Geomech. Eng.*, **20**(5), 385-397. https://doi.org/10.12989/gae.2020.20.5.385.

Mozumder, R.A. and Laskar, A.I. (2015), "Prediction of unconfined compressive strength of geopolymer stabilized clayey soil using artificial neural network", *Comput. Geotech.*, **69**, 291-300. https://doi.org/10.1016/j.compgeo.2015.05.021.

Nathan, A.J. and Scobell, A. (2012), "How China sees America", In *Foreign Affairs*, **91**, 191-196. https://doi.org/10.1017/CBO9781107415324.004.

Oh, T.M., Bang, E.S., Cho, G.C. and Park, E.S. (2017), "Estimation of undrained shear strength for saturated clay using shear wave velocity", *Mar. Georesour. Geotec.*, **35**(2), 236-244. https://doi.org/10.1080/1064119X.2016.1140855.

Pooya Nejad, F., Jaksa, M.B., Kakhi, M. and McCabe, B.A. (2009), "Prediction of pile settlement using artificial neural networks based on standard penetration test data", *Comput. Geotech*., **36**(7), 1125-1133. https://doi.org/10.1016/j.compgeo.2009.04.003.

Rahman, M.M., Cubrinovski, M. and Lo, S.R. (2012), "Initial shear modulus of sandy soils and equivalent granular void ratio", *Geomech. Geoeng.*, **7**(3), 219-226. https://doi.org/10.1080/17486025.2011.616935.

Rashidian, M., Ishihara, K., Kokusho, T., Kanatani, M. and Okamoto, T. (1995), "Effect of sample preparation methods on shear wave velocity", *Proceedings of the 2nd International Conference on Seismology and Earthquake Engineering,* Teheran, Iran.

Ruan, B., Miao, Y., Cheng, K. and Yao, E. lei. (2021), "Study on the small strain shear modulus of saturated sand-fines mixtures by bender element test", *Eur. J. Enviro. Civil Eng.*, **25**(1), 28-38. https://doi.org/10.1080/19648189.2018.1513870.

Saadat, M. and Bayat, M. (2022), "Prediction of the unconfined compressive strength of stabilised soil by Adaptive Neuro Fuzzy Inference System (ANFIS) and Non-Linear Regression (NLR)", *Geomech. Geoeng.*, **17**(1), 80-91. https://doi.org/10.1080/17486025.2019.1699668.

Senetakis, K. and Payan, M. (2018), "Small strain damping ratio of sands and silty sands subjected to flexural and torsional resonant column excitation", *Soil Dyn. Earthq. Eng.*, **114**, 448-459. https://doi.org/10.1016/j.soildyn.2018.06.010.

Shirley, D.J. (1978), "An improved shear wave transducer", *J. Acoust. Soc. Am.*, **63**(5), 1643-1645. https://doi.org/10.1121/1.381866.

Sihag, P., Tiwari, N.K. and Ranjan, S. (2019), "Prediction of unsaturated hydraulic conductivity using adaptive neuro- fuzzy inference system (ANFIS)", *ISH J. Hydraulic Eng.*, **25**(2), 132-142. https://doi.org/10.1080/09715010.2017.1381861.

Sivapullaiah, P.V., Guru Prasad, B. and Allam, M.M. (2009), "Modeling sulfuric acid induced swell in carbonate clays using artificial neural networks", *Geomech. Eng.*, **1**(4), 307-321. https://doi.org/10.12989/gae.2009.1.4.307.

Teachavorasinskun, S. and Pongvithayapanu, P. (2016), "Shear wave velocity of sands subject to large strain triaxial loading", *Geomech. Eng.*, **11**(5), 713–723. https://doi.org/10.12989/gae.2016.11.5.713.

Ueno, K., Kuroda, S., Hori, T. and Tatsuoka, F. (2019), "Elastic shear modulus variations during undrained cyclic loading and subsequent reconsolidation of saturated sandy soil", *Soil Dyn. Earthq. Eng.*, **116**, 476-489. https://doi.org/10.1016/j.soildyn.2018.10.041.

Wang, G.X. and Kuwano, J. (1999), "Modeling of strain dependency of shear modulus and damping of clayey sand", *Soil Dyn. Earthq. Eng.*, **18**(6), 463-471. https://doi.org/10.1016/S0267-7261(99)00010-X.

Wichtmann, T., Navarrete Hernández, M.A. and Triantafyllidis, T. (2015), "On the influence of a non-cohesive fines content on small strain stiffness, modulus degradation and damping of quartz sand", *Soil Dyn. Earthq. Eng.*, **69**, 103-114. https://doi.org/10.1016/j.soildyn.2014.10.017.

Xiao, H., Yao, K., Liu, Y., Goh, S.H. and Lee, F.H. (2018), "Bender element measurement of small strain shear modulus of cement-treated marine clay – Effect of test setup and methodology", *Constr. Build. Mater.*, **172**, 433-447. https://doi.org/10.1016/j.conbuildmat.2018.03.258.

Yamada, S., Hyodo, M., Orense, R.P. and Dinesh, S.V. (2008), "Initial shear modulus of remolded sand-clay mixtures", *J. Geotech. Geoenviron. Eng.*, **134**(7), 960-971. https://doi.org/10.1061/(asce)1090-0241(2008)134:7(960).

Yang, J. and Yan, X.R. (2009), "Factors affecting site response to multi-directional earthquake loading", *Eng. Geol.*, **107**(3-4), 77-87. https://doi.org/10.1016/j.enggeo.2009.04.002.

Yang, Z.X., Lit, X.S., Yang, J., Li, X.S. and Yang, J. (2008), "Quantifying and modelling fabric anisotropy of granular soils", *Geotechnique*, **58**(4), 237-248. https://doi.org/10.1680/geot.2008.58.4.237.

Youn, J.U.U., Choo, Y.W.W. and Kim, D.S.S. (2008), "Measurement of small-strain shear modulus Gmax of dry and saturated sands by bender element, resonant column, and

torsional shear tests", *Can. Geotech. J.*, **45**(10), 1426–1438. https://doi.org/10.1139/T08-069.

Yu, P. and Richart, F.E. (1984), "Stress ratio effects on shear modulus of dry sands", *J. Geotech. Eng.*, **110**(3), 331-345. https://doi.org/10.1061/(ASCE)0733-9410(1984)110:3(331).

Zhou, Z., Yang, H., Xing, K. and Gao, W. (2018), "Prediction models of the shear modulus of normal or frozen soil-rock mixtures", *Geomech. Eng.*, **15(**2), 783-791. https://doi.org/10.12989/gae.2018.15.2.783.

Zhu, S., Yang, G., Wen, Y. and Ou, L. (2014), "Dynamic shear modulus reduction and damping under high confining pressures for gravels", *Geotech. Lett.*, **4**, 179-186. https://doi.org/10.1680/geolett.14.00030.

GC